



Effect of Discontinuous Yielding on the Strain Hardening Behavior of Fine-Grained Twinning-Induced Plasticity Steel

Singon Kang^{1*}, Sujin Jeong¹ and Yeon-Sang Ahn²

¹Department of Materials Science and Engineering, Dong-A University, Busan, Republic of Korea, ²Technical Research Laboratories, POSCO, Gwangyang, Republic of Korea

OPEN ACCESS

Edited by:

John Gordon Speer,
Advanced Steel Processing and
Products Research Center (ASPPRC),
United States

Reviewed by:

Mingxin Huang,
The University of Hong Kong,
Hong Kong
Ricardo Emilio Aristizabal-Sierra,
University of Antioquia, Colombia

*Correspondence:

Singon Kang
skang@dau.ac.kr

Specialty section:

This article was submitted to
Structural Materials,
a section of the journal
Frontiers in Materials

Received: 27 August 2020

Accepted: 19 January 2021

Published: 12 April 2021

Citation:

Kang S, Jeong S and Ahn Y-S (2021)
Effect of Discontinuous Yielding on the
Strain Hardening Behavior of Fine-
Grained Twinning-Induced
Plasticity Steel.
Front. Mater. 8:599534.
doi: 10.3389/fmats.2021.599534

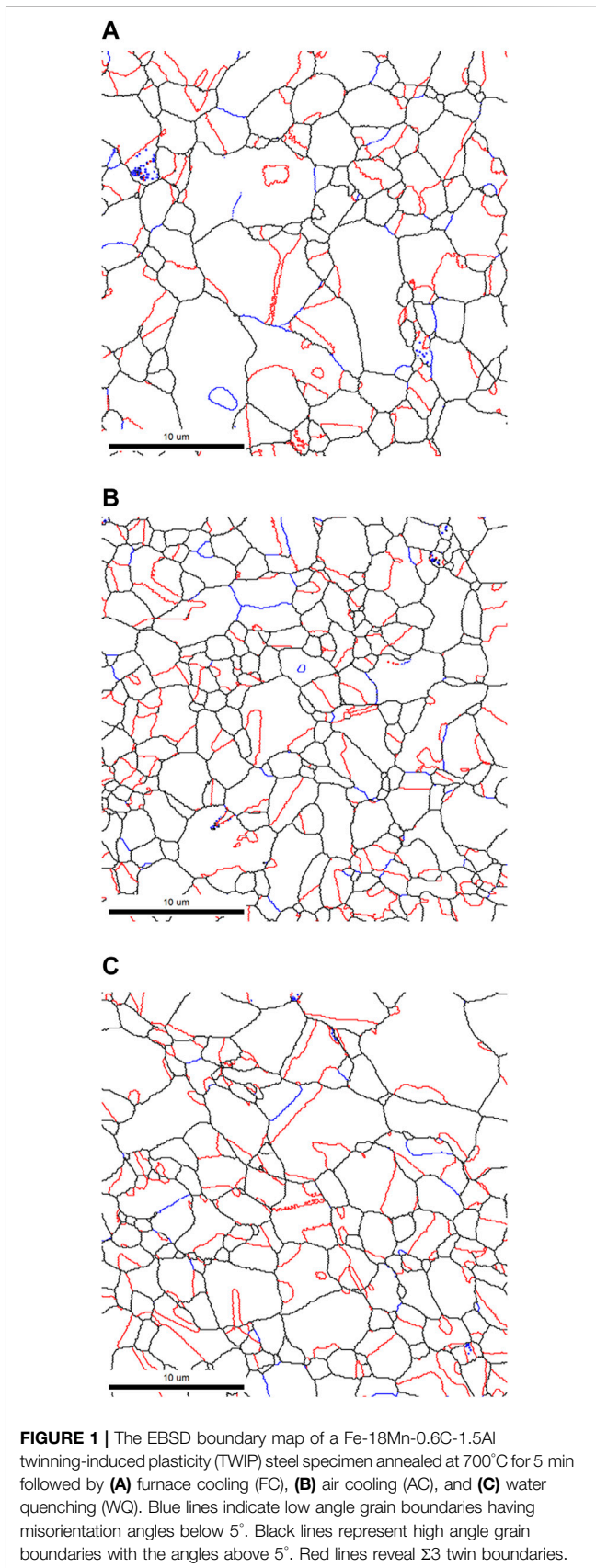
The yielding of a high Mn twinning-induced plasticity steel was examined in three fine-grained specimens recrystallized at 700°C for 5 min with different cooling conditions. While the stress-strain curves of furnace-cooled and air-cooled specimens exhibit a stress drop at yielding, the drop was not observed in the water-quenched specimen. A simple analysis of the displacement data indicates the occurrence of localized deformation at the beginning of the plastic deformation in the three tensile specimens with different cooling conditions. The localized deformation of all three specimens was confirmed as Lüders strain by digital image correlation (DIC) analysis. Based on this observation, the role of yielding behavior on the strain hardening rate evolution at an early stage of the tensile deformation was discussed.

Keywords: advanced high strength steels, austenitic steels, twinning-induced plasticity steel, yield phenomena, discontinuous yielding, work hardening, ultrafine grained microstructure

INTRODUCTION

Twinning-induced plasticity (TWIP) steel is one of the representative austenitic steels developed originally for formable automotive sheet applications (Kim et al., 1989; Grässel et al., 2000). Due to the deformation twinning, a large strain hardening is known to be available in the high Mn austenitic steel, resulting in attractive combinations of ultimate tensile strength (UTS) and total elongation (TE) (Bouaziz and Guelton, 2001; Gil Sevillano, 2009). However, in other austenitic steels and austenitic ferrous alloys, a low yield strength (YS) is regarded as a representative drawback of the TWIP steel (Bouaziz et al., 2011; Yan et al., 2012; Diao et al., 2017).

Considering conventional production process of cold-rolled sheet steel, additional strengthening of the TWIP steel is available by grain refinement (Kang et al., 2010; Saha et al., 2013). Including the strength level, diverse tensile deformation characteristics of the TWIP steel are influenced by the grain refinement, and it affects the strain hardening behavior (Dini et al., 2010; Gutierrez-Urrutia et al., 2010; Dini and Ueji, 2012; Gutierrez-Urrutia and Raabe, 2012). First, deformation twinning is reduced during the tensile deformation of the fine-grained TWIP steel (Ueji et al., 2008; Kang et al., 2016; Mohammadzadeh and Mohammadzadeh, 2019; Hwang, 2020). Reversely, its dislocation accumulation kinetics is accelerated (Jeong et al., 2011). It results in a higher strain hardening rate (SHR) at small strains in the fine-grained specimen than in the coarse-grained specimen, whereas the rate is reversed with further strain (Gutierrez-Urrutia and Raabe, 2012; Kang et al., 2016; Tian et al., 2017). Although the total strain hardening capability does not vary much with the grain size, the higher SHR maintained to the large strain region in the coarse-grained specimen improves its ductility.



The yielding behavior of the TWIP steel is also dependent significantly on the austenite grain size. Almost all coarse-grained TWIP steels exhibit stress-strain curves including continuous yielding behavior. Meanwhile, although this phenomenon is rarely discussed, the yielding sections of the stress-strain curves of TWIP steels having an average grain size smaller than 10 μm usually exhibit discontinuous yielding characteristics (Uejii et al., 2008; Dini et al., 2010; Kang et al., 2016; Gwon et al., 2020). A similar dependence of the yielding behavior on the grain size can be found in diverse metals and alloys including steels and Fe-based alloys having an austenite single phase microstructure (Tsuji et al., 2002; Yu et al., 2005; Poling, 2012; Sun et al., 2018).

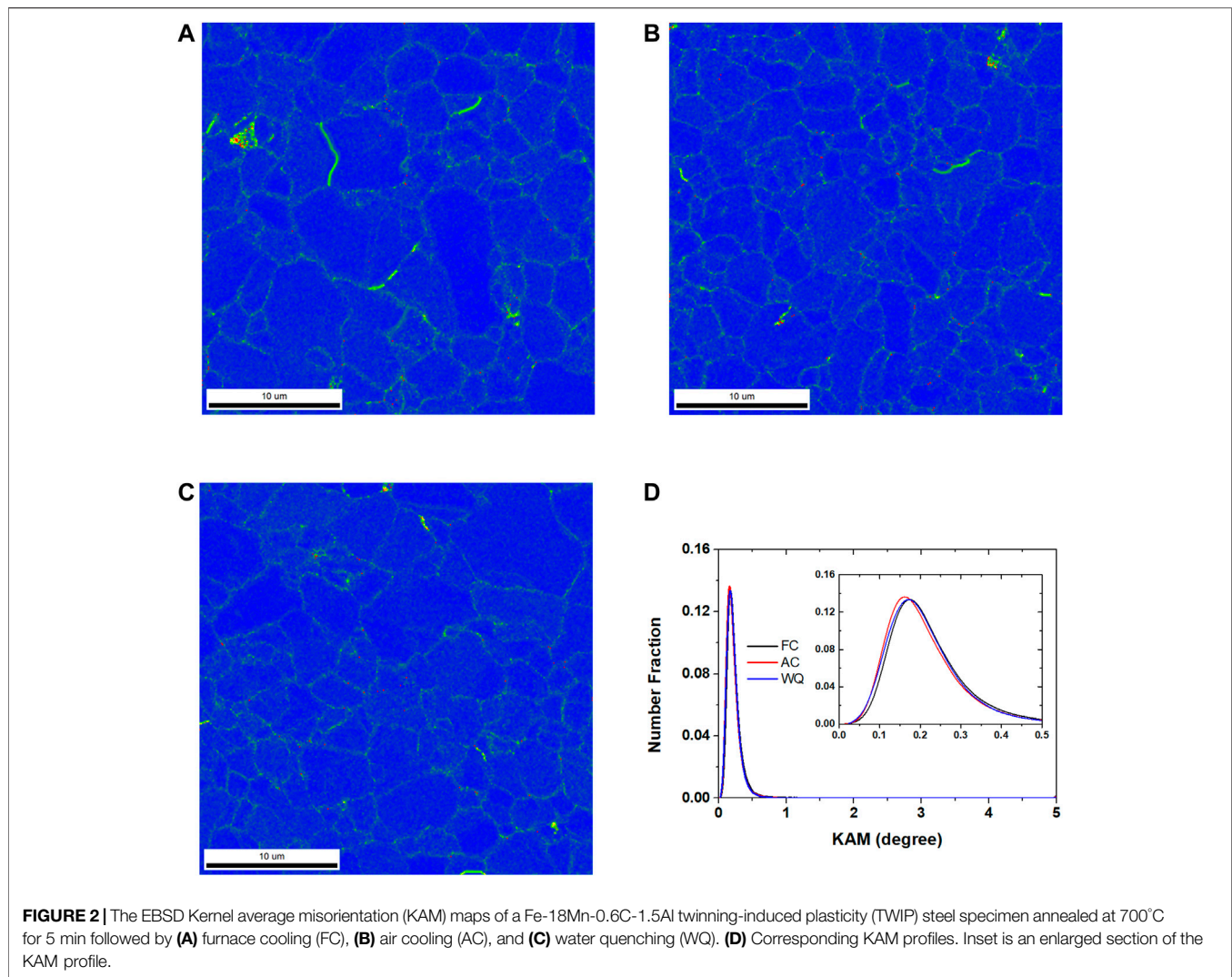
Due to the transition of the yielding characteristics, the strain hardening behavior of the fine-grained TWIP steel in particular at the initial stage of the tensile deformation is also different from the coarse-grained one. A small strain range of negative value and its following sharp increase in the yielding section of the SHR ($d\sigma/d\varepsilon$) vs. true strain (ε) curve was reported from the Fe-18Mn-0.6C-1.5Al TWIP steel with the grain size of 2 μm , whereas the valley-type fluctuation of the SHR was not observed in the coarse-grained specimen exhibiting continuous yielding behavior (Kang et al., 2016). The discontinuous yielding is regarded again as the origin of the similar valley-type fluctuation of the ($d\sigma/d\varepsilon$) vs. ε curve in the early stage of tensile deformation in the Fe-22Mn-0.6C steel having a grain size of 0.6 μm (Tian et al., 2017).

Although the similar increase of the SHR about 1,000 MPa or more at the initial stage of the tensile deformation is frequently observed in fine-grained TWIP steels, discontinuous yielding is not regarded as its principal cause (Madivala and Bleck, 2019; Gwon et al., 2020). Rather, since the analysis of the strain hardening behavior with stages, it is generally interpreted as a result of the onset of deformation twinning, corresponding to “stage B” (Barbier et al., 2009). While the positive contribution of deformation twinning to the SHR values is a well-known and experimentally verified phenomenon, the application of this interpretation to the analysis of the rapid increase of the SHR value about 1,000 MPa within a short range of the true strain, an extremely accelerated deformation twinning is required. However, considering their grain size corresponding deformation twinning kinetics only in the fine-grained TWIP steel does not seem to be reasonable.

The analysis of the strain hardening behavior of the fine-grained TWIP steel without consideration of the yielding is probably due to the difficulties of identifying the discontinuous yielding from the stress-strain curves. However, for a comprehensive understanding of the strain hardening behavior in the fine-grained TWIP steel, the contribution of the discontinuous yielding is required to be examined. Thus, the objective of the present study is to examine detailed yielding behavior of fine-grained TWIP steel and to explain its effect on the strain hardening behavior.

EXPERIMENTAL PROCEDURE

A 30 kg ingot of the TWIP steel with the size of 220 \times 170 \times 100 mm³ was prepared by vacuum induction melting and



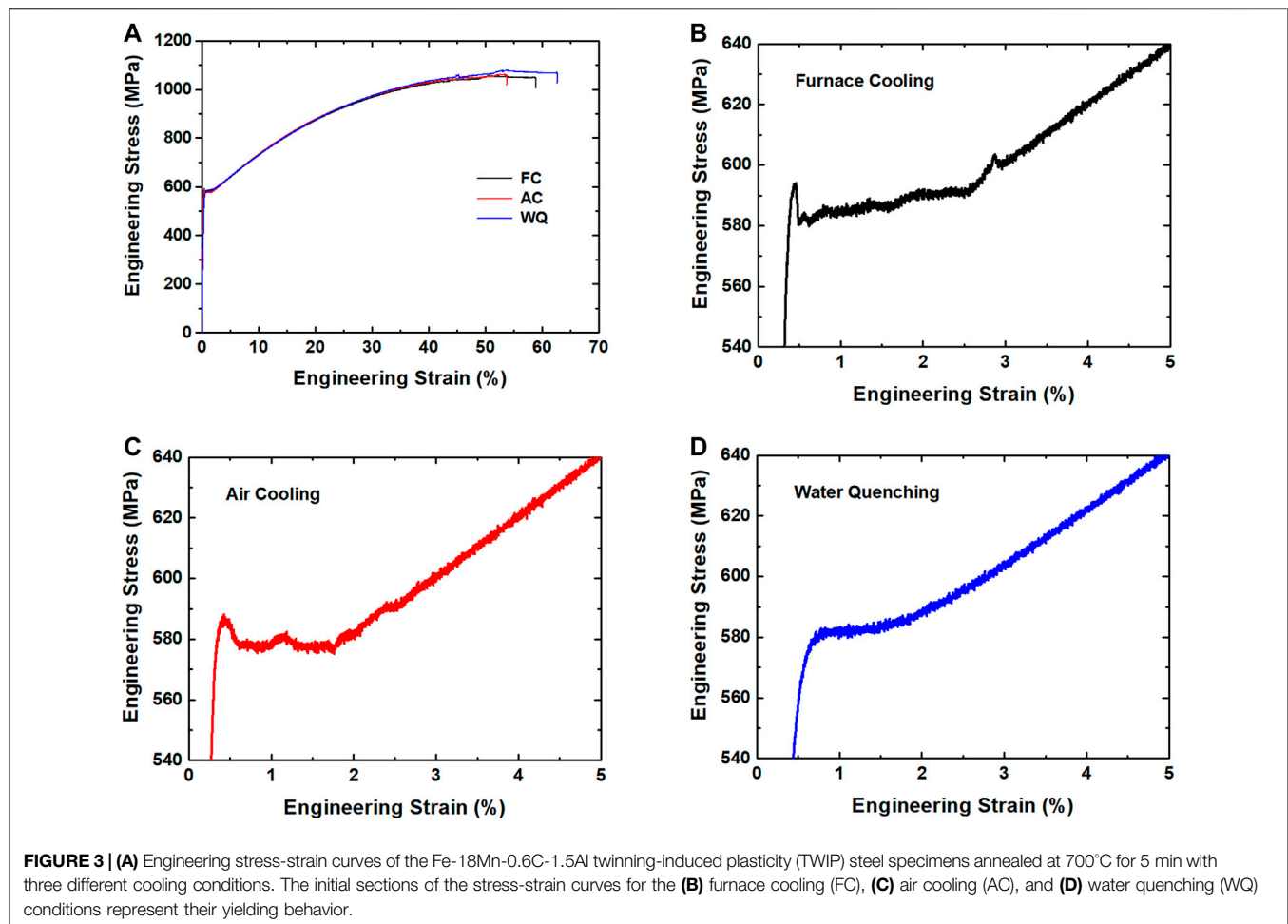
laboratory cast, whose chemical composition measured by OES spectrometer is Fe-18.22Mn-0.60C-1.55Al in wt%. After homogenization heat treatment at 1,200°C for 1 h, the ingot was hot rolled to a plate with a final thickness of 3 mm followed by furnace cooling to room temperature. The plate was cold rolled with a reduction ratio of 60%. The thickness of the cold-rolled sheet is 1.2 mm. Using a vacuum tube furnace (LHA-12/300, Lenton Thermal Designs Limited, Hope Valley, United Kingdom), the sheet was annealed at 700°C for 5 min and cooled in three different conditions, i.e., furnace cooling (FC), air cooling (AC), and water quenching (WQ) to obtain a set of samples with different yielding behavior.

Microstructural observations of the WQ specimen were carried out using a field emission gun scanning electron microscope (FEG-SEM, Inspect F50, FEI, Hillsboro, OR, United States) equipped with an electron backscatter diffraction (EBSD, Hikari, EDAX, Mahwah, NJ, United States). Samples for the EBSD observation were prepared by mechanical polishing process finalized with an aqueous solution containing 0.04 μm colloidal silica particles. The FEG-SEM was operated at

20 keV with a working distance of 20 mm. Multiple EBSD maps having a scan area of 30 μm × 30 μm were obtained at a magnification of 3,000× with a step size of 0.1 μm on a hexagonal grid. The EBSD results were analyzed using TSL OIM Analysis Software 7.

Uniaxial tensile tests were performed at room temperature using a computer controlled hydraulic mechanical testing machine (MTS 810, MTS Inc., Eden Prairie, MN, United States). The samples were prepared as ASTM-E8M rectangular subsize specimen with a gauge length of 25 mm (ASTM Standard, 2011). In each cooling condition, more than three samples were tested. Tensile axis of the specimen is parallel to the rolling direction of the annealed sheets. To perform the tensile test under a constant strain rate of $1 \times 10^{-3} \text{ s}^{-1}$, the strain for the 25 mm gauge section was measured using an axial extensometer (model 632.24-50, MTS Inc., Eden Prairie, MN, United States).

To examine localized characteristics of the deformation related to the yielding, digital image correlation (DIC, VIC-2D, Correlated Solutions, Irmo, SC, United States) method



was applied. The tensile specimens were prepared with a surface covered with a random speckle pattern for the analysis. Ten frames of the surface images were obtained per second. Based on the evolutions of the surface images, the distribution of uniaxial tensile strain along the tensile axis was examined.

RESULTS AND DISCUSSION

Fully recrystallized polygonal grain structure of the Fe-18Mn-0.6C-1.5Al TWIP steel specimen annealed at 700°C for 5 min with the three different cooling conditions was observed from the EBSD boundary map as shown in **Figure 1**. Blue, black, and red lines indicate low angle ($<5^\circ$), high angle ($>5^\circ$), and twin boundaries. The average grain size of the austenite is about 1.8 μm . Corresponding Kernel average misorientation (KAM) maps for the FC, AC, and WQ samples were shown in **Figures 2A,B,C, 2**, respectively. The almost identical KAM profiles of the three samples provided in **Figure 2D** indicate a negligible difference of the grain structure for the three TWIP steel specimens.

The tensile stress-strain curves of the TWIP steel specimens annealed at 700°C for 5 min with three different cooling

conditions (FC, AC, and WQ) shown in **Figure 3A** are almost indistinguishable to each other. The YS and UTS values of the three specimens are approximately 580 MPa and 1,050 MPa, respectively. The TE values for the three specimens are about 60%. As shown in the microstructural observation results, because the specimens were fully recrystallized by the holding at 700°C for 5 min, the following cooling conditions should have a limited effect on the tensile properties.

Meanwhile, the yielding section of the stress-strain curves is dependent largely on the cooling conditions. The enlarged stress-strain curve of the FC specimen in **Figure 3B** shows a sharp stress drop at an engineering strain of 0.5%, which includes upper and lower yield points. The stress levels of the upper yield point and the lower yield point are 594 MPa and 580 MPa, respectively. After the stress peak, the curve fluctuates to the engineering strain of 3%, corresponding to yield point elongation. These are representative features of a discontinuous yielding behavior.

The degree of discontinuous yielding characteristics becomes reduced with increasing cooling rate. While the signals related to the discontinuous yielding are also observed in the tensile curve of the AC specimen, the yield point peak is blunted and the strain range for the yield point elongation narrows down (**Figure 3C**). The yielding of the WQ specimen provided in **Figure 3D** is

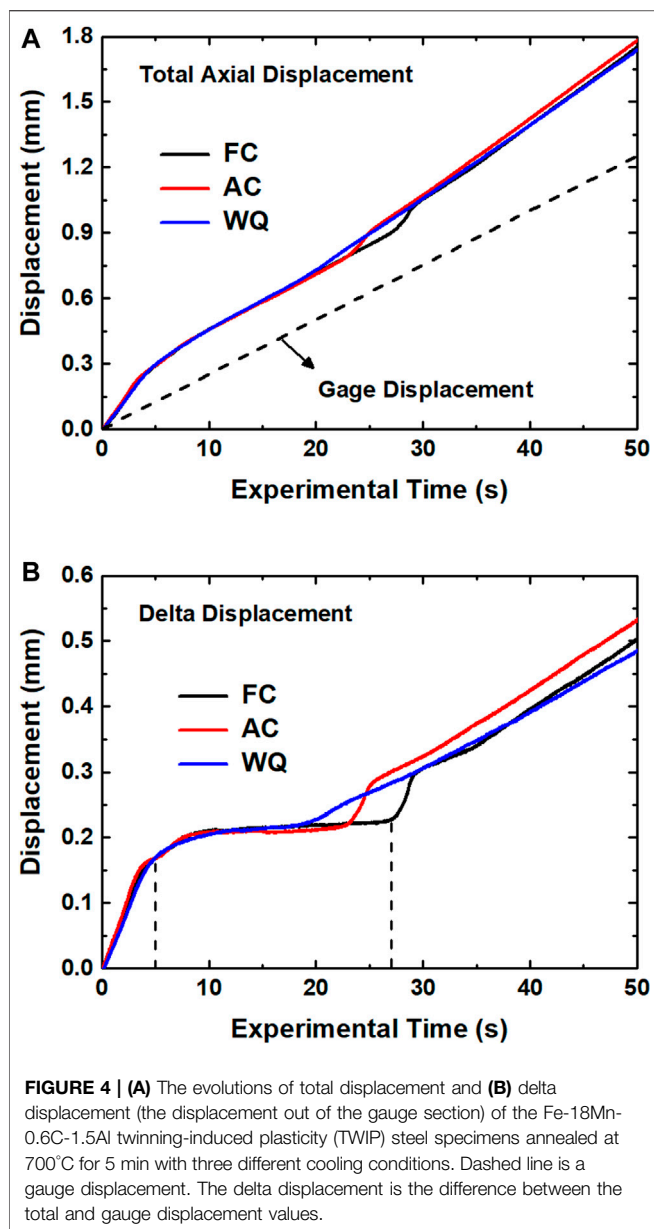


FIGURE 4 | (A) The evolutions of total displacement and **(B)** delta displacement (the displacement out of the gauge section) of the Fe-18Mn-0.6C-1.5Al twinning-induced plasticity (TWIP) steel specimens annealed at 700°C for 5 min with three different cooling conditions. Dashed line is a gauge displacement. The delta displacement is the difference between the total and gauge displacement values.

somewhat ambiguous to define its characteristics based on the tensile stress-strain curve. It does not reveal the upper and lower yield points in the stress-strain curve.

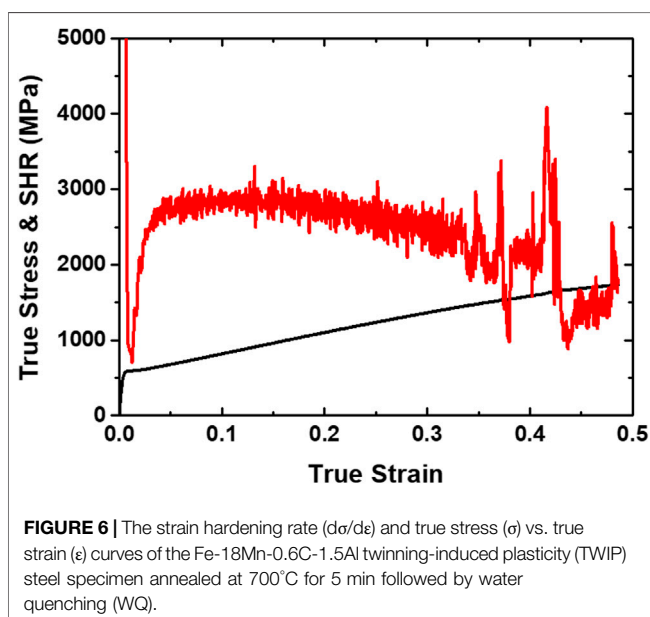
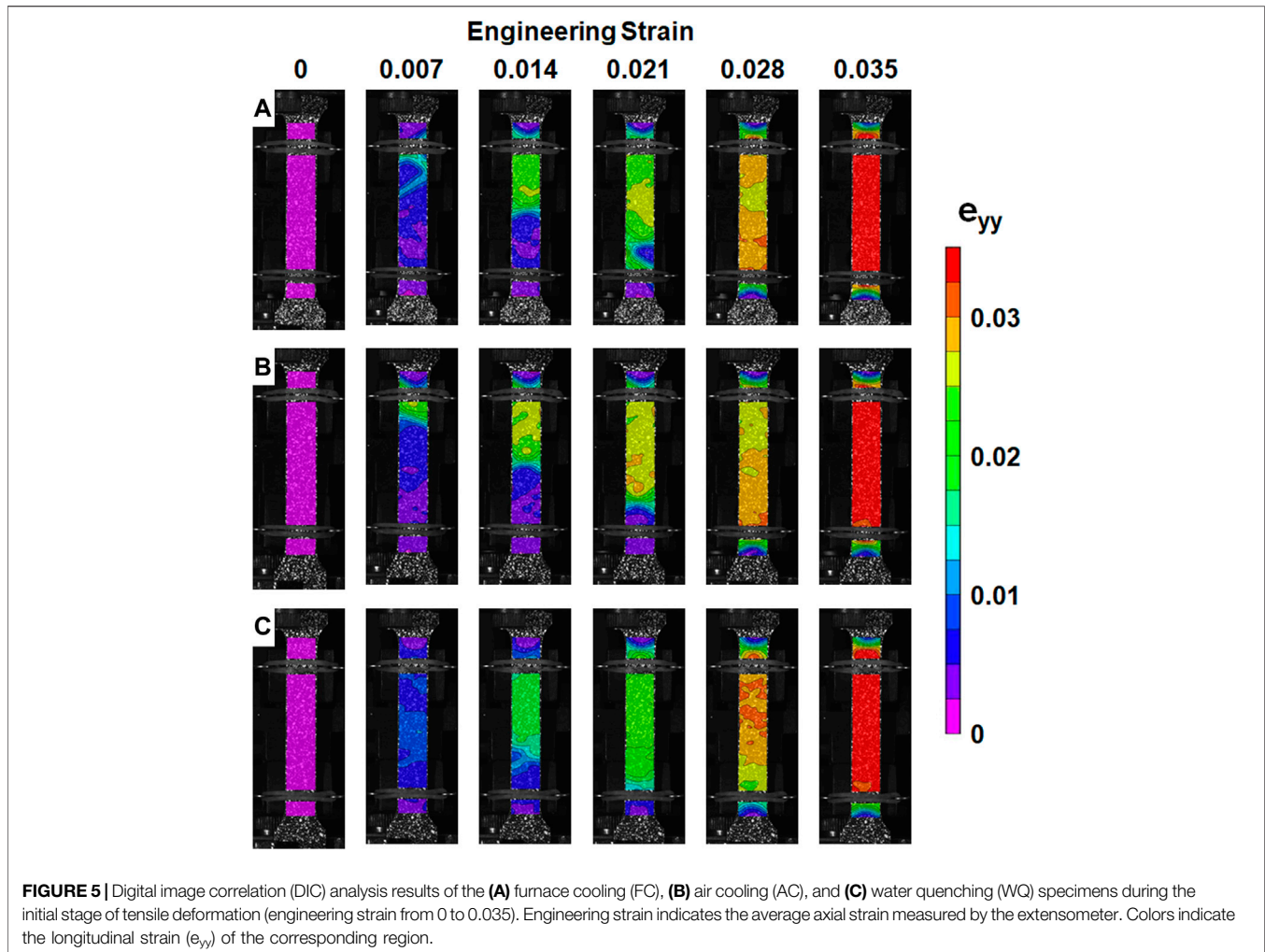
While the microstructures of the three samples including degree of recrystallization and grain structure are almost identical, there should be a difference of the dislocation mobility. With slower cooling rates, more pinning of dislocations by solute carbon atoms is available in the FC specimen. It possibly results in more discontinuous characteristics in the yielding behavior. To further scrutinize the yielding behavior of the three specimens, a simple analysis of the displacement data was carried out. Initial sections of the sample displacement vs. experimental time plots for the three cooling conditions were shown in **Figure 4A**. Total displacement indicates the axial displacement of the entire specimen measured

from the MTS 810 machine, and the gauge displacement is the displacement corresponding to the gauge section (25 mm) measured from the extensometer. The gauge displacement increases linearly with the experimental time and independent of the sample cooling conditions, because the tensile testing of the three specimens was carried out in the same strain rate ($1 \times 10^{-3} \text{ s}^{-1}$) condition. However, the evolution of the total displacement varies with the sample cooling conditions.

Regarding the shape of the specimen (ASTM E8M rectangular subsize specimen), the 32-mm-long section in the middle of the specimen has the minimum but uniform cross-sectional area, referred to as reduced section. Gauge section (25 mm in length) is a central part of the reduced section. Even excluding the end of the reduced section where stress concentration occurs, part of the reduced section, which does not belong to the gauge section, can be deformed in the same strain rate condition as the gauge section. Thus, the increasing rate of the total displacement, the slope of the total displacement vs. experimental time plot, is required to be greater than the rate of the gauge displacement. However, as shown in **Figure 4A**, this is not always true.

Figure 4B shows the evolution of the difference between the total displacement and gauge displacement values, referred to as delta displacement, representing the displacement out of the gauge section. The delta displacement plot can be divided into three sections based on its slope change. Two vertical dashed lines in **Figure 4B** indicate the boundaries between the three sections in the plot of the FC specimen. In the first section, the delta displacement values increase proportionally to the gauge displacement. This section corresponds to the strain range for the uniform elastic deformation prior to the yielding. The second section of the delta displacement plot reveals a deformation localized in the gauge section, indicating a propagation of Lüders band through the gauge section. The rapid increase of the delta displacement at the beginning of the third section seems to be due to the propagation of the Lüders band out of the gauge section. To maintain the given strain rate of the gauge section without the band, stress level is required to be increased rapidly, which corresponds to the stress evolution at a strain of 3% observed in **Figure 3B**. It results in a faster propagation of the Lüders band to its end. The following linear section of the delta displacement represents the uniform plastic deformation after the end of the Lüders band propagation.

It is worth mentioning that the WQ specimen having no clear signal of discontinuous yielding in the stress-strain curve shows a strain range for localized deformation during yielding in the delta displacement analysis. To verify the deformation characteristics during yielding, DIC analysis was performed and the results were provided in **Figure 5**. As well as the results of the FC (**Figure 5A**) and AC (**Figure 5B**) specimens, the strain distribution maps of the WQ specimen in **Figure 5C** show a nonuniform distribution of strain during yielding. In that sequential strain distribution maps, the Lüders band is nucleated from the upper section of the gauge and propagated to the lower sections. At an engineering strain of 0.014, all three samples exhibit uneven distribution of the strain in the gauge section, indicating the propagation of the Lüders band. In that condition, the strain out of the gauge section is limited. With strains of over 0.028, the strain in the gauge



section becomes almost uniform, representing that the uniform plastic deformation is started after the full propagation of Lüders band along the gauge section. It also accompanies the plastic deformation out of the gauge section. This analysis corresponds well to the analysis from the delta displacement result in **Figure 4B**.

Corresponding ($d\sigma/d\varepsilon$) vs. ε curve of the WQ specimen is shown in **Figure 6**. The SHR value is dropped to about 800 MPa and recovered rapidly to 2,800 MPa within a true strain of 0.05, showing a valley-type evolution. After the valley, the SHR value decreases gradually to the true strain of 0.3, and it fluctuated largely due to the serrations in the further strain range. This valley-type strain hardening behavior at an early stage of the tensile deformation has been reported repeatedly in diverse TWIP steels having an average grain size mostly below 10 μm (Tian et al., 2017; Madivala and Bleck, 2019; Gwon et al., 2020). While the level of the SHR in the valley region varies with the experimental conditions, the gap between the levels of the lower and upper bounds of the valley is about 1,000 MPa or greater in many samples.

As mentioned earlier, the explosive increase of the SHR at a short strain range around the yielding section is commonly

interpreted as a result of the onset of deformation twinning (Barbier et al., 2009). However, even though the tensile deformation behavior does not meet the Considère criterion ($d\sigma/d\epsilon < \sigma$) at the early stage of the tensile deformation, there is a localized deformation in that strain range, whose effect should be taken into account in the analysis of the corresponding strain hardening behavior. During the propagation of Lüders band, the density of dislocations in the local deforming area can be maintained to be constant. While the plastic deformation increases the density of dislocations in the deforming area, it should be considered that the propagation of the band is toward the undeformed area. As a result, the strain range for the Lüders band propagation exhibits a negligible amount of strain hardening. It explains the lower section of the valley-type SHR evolution. Meanwhile, with the beginning of the uniform plastic deformation, the dislocation density of the deformation region increases gradually with strain, resulting in a higher SHR value. The different deformation behavior between the Lüders band propagation and uniform plastic deformation regions provides a short strain range for the rapid increase of the SHR value, corresponding to the right side of the valley-type SHR evolution. Thus, the shape of the SHR valley is influenced by the yielding characteristics. For this reason, the analysis of the strain hardening behavior of a fine-grain TWIP steel requires a more comprehensive approach with considering the yielding behavior.

CONCLUSION

In summary, the yielding behavior of a twinning-induced plasticity steel was examined in the samples recrystallized at

REFERENCES

- ASTM Standard (2011). *E8/E8M Standard test methods for tension testing of metallic materials*. West Conshohocken, PA: ASTM International, Vol. 3, 66.
- Barbier, D., Gey, N., Allain, S., Bozzolo, N., and Humbert, M. (2009). Analysis of the tensile behavior of a TWIP steel based on the texture and microstructure evolutions. *Mater. Sci. Eng. A* 500, 196–206. doi:10.1016/j.msea.2008.09.031
- Bouaziz, O., Allain, S., Scott, C. P., Cugy, P., and Barbier, D. (2011). High manganese austenitic twinning induced plasticity steels: a review of the microstructure properties relationships. *Curr. Opin. Solid State Mater. Sci.* 15, 141–168. doi:10.1016/j.cossms.2011.04.002
- Bouaziz, O., and Guelton, N. (2001). Modelling of TWIP effect on work-hardening. *Mater. Sci. Eng. A* 319, 246–249. doi:10.1016/s0921-5093(00)02019-0
- Diao, H. Y., Feng, R., Dahmen, K. A., and Liaw, P. K. (2017). Fundamental deformation behavior in high-entropy alloys: an overview. *Curr. Opin. Solid State Mater. Sci.* 21, 252–266. doi:10.1016/j.cossms.2017.08.003
- Dini, G., Najafzadeh, A., Ueji, R., and Monir-Vaghefi, S. M. (2010). Tensile deformation behavior of high manganese austenitic steel: the role of grain size. *Mater. Des.* 31, 3395–3402. doi:10.1016/j.matdes.2010.01.049
- Dini, G., and Ueji, R. (2012). Effect of grain size and grain orientation on dislocations structure in tensile strained TWIP steel during initial stages of deformation. *Steel Res. Int.* 83, 374–378. doi:10.1002/srin.201100308
- Gil Sevillano, J. (2009). An alternative model for the strain hardening of FCC alloys that twin, validated for twinning-induced plasticity steel. *Scr. Mater.* 60, 336–339. doi:10.1016/j.scriptamat.2008.10.035
- 700°C for 5 min with three different cooling conditions. While furnace-cooled and air-cooled specimens exhibit a stress drop and following Lüders strain, the stress-strain curve of the water-quenched specimen does not have the signals of discontinuous yielding. However, both a simple displacement analysis and DIC analysis confirmed that Lüders band is commonly formed and propagated in the three specimens. As a result of the localized deformation and following transition to the uniform plastic deformation, a valley-type evolution of the strain hardening rate is observed at an early stage of the tensile deformation.

DATA AVAILABILITY STATEMENT

The original contributions presented in the study are included in the article/Supplementary Material; further inquiries can be directed to the corresponding author.

AUTHOR CONTRIBUTIONS

SK organized the experiments and wrote the manuscript. SJ performed the experiments and following analysis. YA contributed to the design of experiments and edited the manuscript.

FUNDING

This work was supported by the Dong-A University research fund.

- Grässel, O., Krüger, L., Frommeyer, G., and Meyer, L. W. (2000). High strength Fe-Mn-(Al, Si) TRIP/TWIP steels development—properties—application. *Int. J. Plast.* 16, 1391–1409. doi:10.1016/s0749-6419(00)00015-2
- Gutierrez-Urrutia, I., and Raabe, D. (2012). Grain size effect on strain hardening in twinning-induced plasticity steels. *Scr. Mater.* 66, 992–996. doi:10.1016/j.scriptamat.2012.01.037
- Gutierrez-Urrutia, I., Zaefferer, S., and Raabe, D. (2010). The effect of grain size and grain orientation on deformation twinning in a Fe-22wt.% Mn-0.6wt.% C TWIP steel. *Mater. Sci. Eng. A* 527, 3552–3560. doi:10.1016/j.msea.2010.02.041
- Gwon, H., Kim, J. H., Kim, J.-K., Suh, D.-W., and Kim, S.-J. (2020). Role of grain size on deformation microstructures and stretch-flangeability of TWIP steel. *Mater. Sci. Eng. A* 773, 138861. doi:10.1016/j.msea.2019.138861
- Hwang, J.-K. (2020). Effect of grain size on tensile and wire drawing behaviors in twinning-induced plasticity steel. *Mater. Sci. Eng. A* 772, 138709. doi:10.1016/j.msea.2019.138709
- Jeong, J. S., Koo, Y. M., Jeong, I. K., Kim, S. K., and Kwon, S. K. (2011). Microstructural study of high-Mn TWIP steels using diffraction profile analysis. *Mater. Sci. Eng. A* 530, 128–134. doi:10.1016/j.msea.2011.09.060
- Kang, S., Jung, J.-G., Kang, M., Woo, W., and Lee, Y.-K. (2016). The effects of grain size on yielding, strain hardening, and mechanical twinning in Fe-18Mn-0.6 C-1.5 Al twinning-induced plasticity steel. *Mater. Sci. Eng. A* 652, 212–220. doi:10.1016/j.msea.2015.11.096
- Kang, S., Jung, Y.-S., Jun, J.-H., and Lee, Y.-K. (2010). Effects of recrystallization annealing temperature on carbide precipitation, microstructure, and mechanical properties in Fe-18Mn-0.6 C-1.5 Al TWIP steel. *Mater. Sci. Eng. A* 527, 745–751. doi:10.1016/j.msea.2009.08.048

- Kim, Y. G., Han, J. M., and Lee, J. S. (1989). Composition and temperature dependence of tensile properties of austenitic FeMnAlC alloys. *Mater. Sci. Eng. A* 114, 51–59. doi:10.1016/0921-5093(89)90844-7
- Madivala, M., and Bleck, W. (2019). Strain rate dependent mechanical properties of TWIP steel. *JOM* 71, 1291–1302. doi:10.1007/s11837-018-3137-0
- Mohammadzadeh, R., and Mohammadzadeh, M. (2019). Inverse grain size effect on twinning in nanocrystalline TWIP steel. *Mater. Sci. Eng. A* 747, 265–275. doi:10.1016/j.msea.2018.11.085
- Poling, W. A. (2012). Grain size effects in micro-tensile testing of austenitic stainless steel. Master's thesis. Golden (CO): Colorado School of Mines.
- Saha, R., Ueji, R., and Tsuji, N. (2013). Fully recrystallized nanostructure fabricated without severe plastic deformation in high-Mn austenitic steel. *Scr. Mater.* 68, 813–816. doi:10.1016/j.scriptamat.2013.01.038
- Sun, S., Tian, Y., Lin, H., Yang, H., Dong, X., Wang, Y., et al. (2018). Transition of twinning behavior in CoCrFeMnNi high entropy alloy with grain refinement. *Mater. Sci. Eng. A* 712, 603–607. doi:10.1016/j.msea.2017.12.022
- Tian, Y., Bai, Y., Zhao, L., Gao, S., Yang, H., Shibata, A., et al. (2017). A novel ultrafine-grained Fe₂₂Mn₀.6C TWIP steel with superior strength and ductility. *Mater. Charact.* 126, 74–80. doi:10.1016/j.matchar.2016.12.026
- Tsuji, N., Ito, Y., Saito, Y., and Minamino, Y. (2002). Strength and ductility of ultrafine grained aluminum and iron produced by ARB and annealing. *Scr. Mater.* 47, 893–899. doi:10.1016/s1359-6462(02)00282-8
- Ueji, R., Tsuchida, N., Terada, D., Tsuji, N., Tanaka, Y., Takemura, A., et al. (2008). Tensile properties and twinning behavior of high manganese austenitic steel with fine-grained structure. *Scr. Mater.* 59, 963–966. doi:10.1016/j.scriptamat.2008.06.050
- Yan, F. K., Liu, G. Z., Tao, N. R., and Lu, K. (2012). Strength and ductility of 316L austenitic stainless steel strengthened by nano-scale twin bundles. *Acta Mater.* 60, 1059–1071. doi:10.1016/j.actamat.2011.11.009
- Yu, C. Y., Kao, P. W., and Chang, C. P. (2005). Transition of tensile deformation behaviors in ultrafine-grained aluminum. *Acta Mater.* 53, 4019–4028. doi:10.1016/j.actamat.2005.05.005

Conflict of Interest: The authors declare that the research was conducted in the absence of any commercial or financial relationships that could be construed as a potential conflict of interest.

The handling editor declared a past collaboration with several of the authors (JS).

Copyright © 2021 Kang, Jeong and Ahn. This is an open-access article distributed under the terms of the Creative Commons Attribution License (CC BY). The use, distribution or reproduction in other forums is permitted, provided the original author(s) and the copyright owner(s) are credited and that the original publication in this journal is cited, in accordance with accepted academic practice. No use, distribution or reproduction is permitted which does not comply with these terms.